geosciences

MDPI

Article

Fabrication and Mechanical Evaluation of Eco-Friendly Geopolymeric Mortars Derived from Ignimbrite and Demolition Waste from the Construction Industry in Peru

Fredy Alberto Huamán-Mamani [1,*], Cris Katherin Palomino-Ñaupa [1], María del Mar Orta Cuevas [2] and Santiago Medina-Carrasco [3]

[1] Departamento de Ciencias Naturales, Universidad Católica San Pablo, Arequipa 04001, Peru; ckpalomino@ucsp.edu.pe
[2] Department of Analytical Chemistry, Faculty of Pharmacy, University of Seville, E-41012 Seville, Spain; enmaorta@us.es
[3] X-ray Laboratory (CITIUS), University of Seville, E-41012 Seville, Spain; sanmedi@us.es
* Correspondence: fhuaman@ucsp.edu.pe

Abstract: Ignimbrite rock is a volcanic material located in the Arequipa region (Peru), and for centuries, it has been used as a construction material, giving a characteristic light pastel, white to pink color to the city of Arequipa, with white being the most common. In the present study, the potential use of three types of Arequipa raw materials (ignimbrite rock powder, calcined clay powder, and demolition mortar powder) as the main source of new binders or the manufacture of environmentally friendly mortars, without the addition of ordinary Portland cement (OPC) is discussed. In this work, an in-depth characterization of the materials used was carried out. The proposed fabrication route for geopolymeric materials was considered for the manufacture of binders and mortars using an alkaline solution of NaOH with values between 12 and 18 molar, as a trigger for the geopolymerization process. Geopolymeric mortars were obtained by adding a controlled amount of fine sand to the previously prepared mixture of binder raw material and an alkaline solution. Conventional OPC and geopolymeric mortars manufactured under the same conditions were mechanically evaluated by uniaxial compression tests at a constant compression rate of 0.05 mm/min and under normal conditions of temperature and atmosphere, where the most optimal values were obtained for 15 molar alkaline solutions of ignimbrite without the addition of aggregates, with values of compressive strength of 42 MPa and a modulus elastic of 30 GPa. The results revealed a significant increase in the maximum strength and modulus of elasticity values when the volumetric fractions of OPC are completely replaced with geopolymeric binders in the study conditions of this work, demonstrating the enormous potential of the ignimbrite rock and construction waste studied, as raw material of alternative mortar binders without the addition of OPC. With this work, the ignimbrite rock, of great value in the region and also found in other areas of the Earth's geography, was characterized and valued, in addition to the calcined clay and demolition mortar of the region.

Keywords: ignimbrite; mortar; geopolymer; mechanical strength; binder

check for updates

Citation: Huamán-Mamani, F.A.; Palomino-Ñaupa, C.K.; Orta Cuevas, M.d.M.; Medina-Carrasco, S. Fabrication and Mechanical Evaluation of Eco-Friendly Geopolymeric Mortars Derived from Ignimbrite and Demolition Waste from the Construction Industry in Peru. *Geosciences* **2024**, *14*, 80. https://doi.org/10.3390/geosciences14030080

Academic Editors: Jesus Martinez-Frias, Mohamed Shahin and José Ignacio Alvarez

Received: 13 November 2023
Revised: 13 March 2024
Accepted: 14 March 2024
Published: 15 March 2024

1. Introduction

Ignimbrites are volcanic rocks formed by consolidation of fire cloud particles. Volcanic eruptions expel a large amount of particles of rock fragments, fine glass dust, and gases into the atmosphere, all of which constitute a flammagenitus or fire cloud. When the burning cloud loses the ability to keep the particles in suspension, they fall, forming pyroclastic deposits, which join and form pyroclastic rocks such as ignimbrites. Sillar is the local name given to rocks of the ignimbrite type; the term comes from the region of Arequipa, Peru (Figure 1) [1–3].

Figure 1. Quarry of the Añashuayco deposit, Arequipa, Peru. The figure shows the characteristic color of the ignimbrite rock.

In general, ignimbrite is a material with a porous texture and the ability to absorb liquids and saline solutions without losing its cohesion. It resists heat up to 500 °C without melting. It comes in white, pink, and cream colors. Its moisture absorption reaches 30.8%; it has an average specific weight of 1.65 N/m^3; is a poor conductor of temperature; has resistance to compression of 94.4 kg/cm^2 dry and 85.5 kg/cm^2 wet; its average elastic modulus is 56.875 kg/cm^2 static and 110.05 kg/cm^2 dynamic; and it has high resistance to weathering [1].

Ignimbrites are found throughout the world in volcanic regions that feature high-silica magma and the resulting explosive eruptions. There are known deposits in Australia, New Zealand, Mexico, the United States, and the Canary Islands in Spain. This work focusses on the ignimbrite rock of Peru, where there are many geological units, mainly in Arequipa, Ayacucho, and Puno, which belong to the Cenozoic erathem and are located near volcanoes. The Sencca formation, which allowed for the existence of the main ignimbrite quarries of Arequipa (Peru), consists of rhyolitic composition tuffs that can be distinguished with the naked eye: quartz grains, feldspars, and biotite lamellae. In addition, it contains pumice and lavas that can be rounded or angular and of variable size. They are usually compact. They appear in thick banks and usually show a prismatic disjunction, giving rise to columnar blocks cut by horizontal planes. Two levels are distinguished according to color, one pink to reddish brown and one light grey to white [1]. Currently, in Peru, ignimbrite is georeferenced in the INGEMMET geoscientific database. In 2018, 29 deposits and 14 quarries appeared in this database (Figure 2 and Table 1).

In this work, ignimbrite residues from the Añashuayco ravine (Paccha Quarry, near the Añashuayco deposit) were studied. Paccha quarry (Arequipa) is located in the Cerro Colorado district, province of Arequipa, 10 km in a straight line northwest of the city. The access is by paved road following the Arequipa–Yura route, with a distance of 10.5 km, then 0.5 km by paved road until reaching the Añashuayco ravine (UTM coordinates: 8191 198 N, 222 077 E) [1].

Figure 2. Ignimbrite rock quarry and deposit map (adapted from [1]). Numbering according to codes in Table 1.

The ignimbrite found in this quarry appears as thick banks, without stratification, with vertical scarps due to a prismatic disjunction. Stratigraphically, it belongs to the Añashuayco member of the Sencca volcanic formation. The rock is a white to greyish-white rhyolitic tuff of low specific gravity, compact in large masses and of medium hardness, with quartz crystals, feldspar, inclusions and fragments of andesites, and pumice stones of subangular to subrounded shape. The ignimbrite of this area is exploited along the entire Añashuayco ravine. The exploitation method is open pit, in an artisanal and informal manner. It is important to note that through these methods, a large amount of clearing or waste is generated, contributing to the destruction of natural resources.

Ignimbrite as a material was widely used in colonial times; churches and many public and private civil works were built with it. Currently, it is used in wall covering, in the construction of tourist buildings and walls. It should be noted that of the existing varieties, with shades between white or pink, pink is generally much rarer and more valued, and has generally been used for buildings with high added value, such as churches or monumental buildings.

Between 2000 and 2017, ignimbrite production increased at an average annual rate of 3.9% in Peru with the participation of seven regions, the most important being the Arequipa region with 72%. Ignimbrite consumption is mostly local and is 100% supplied by local production in each of the regions where it exists. It is used as a construction material, in

the cover of facades and architecture, and it is also used as a material to make ornamental figures and monuments [1].

Table 1. Detail of the situation of ignimbrite rock quarries and deposits in Peru ([1], Geoscientific Database—GEOCATMIN).

Code	Region	Province	District	Name	UTM Coordinates		Category
					East	North	
1	Ancash	Bolognesi	Cajacay	Incahuanca	245241	8876224	Deposit
2	Ancash	Recuay	Llacllin	Chaucayan	219806	8872650	Deposit
3	Ancash	Recuay	Marca	Coricoto	229027	8877271	Deposit
4	Ancash	Recuay	Marca	Mogote	224474	8877412	Deposit
5	Apurimac	Antabamba	Antabamba	Mollojo (Wilca)	732995	8406657	Deposit
6	Apurimac	Grau	Mamara	Mamara	759554	8425354	Quarry
7	Arequipa	Arequipa	Cerro Colorado	Flor Blanca	221000	8188994	Deposit
8	Arequipa	Arequipa	Cerro Colorado	La Paccha	222077	8191198	Quarry
9	Arequipa	Arequipa	Majes	Añashuayco	220670	8191105	Deposit
10	Arequipa	Arequipa	Quequeña	El Ingenio II	234960	8169952	Quarry
11	Arequipa	Camana	Ocoña	Lomas Agua Blanca	682514	8201524	Deposit
12	Arequipa	Caravelí	Caravelí	Cantera	682641	8225304	Deposit
13	Arequipa	Caylloma	Huambos	Andaray	730300	8253800	Deposit
14	Ayacucho	Cangallo	Cangallo	Cangallo	593373	8492466	Deposit
15	Ayacucho	Huamanga	Las Nazarenas	Chacco	584212	8553134	Deposit
16	Ayacucho	Huamanga	Pacaycasa	Sillar Ayacuchano	588500	8556620	Deposit
17	Ayacucho	Huanca Sancos	Santiago de Lucanamarca	Lucanamarca	567814	8469314	Deposit
18	Ayacucho	Lucanas	Laramate	Laramate	521412	8420618	Deposit
19	Ayacucho	Víctor Fajardo	Cayara	Mayopampa	612246	8473702	Deposit
20	Cajamarca	Cajamarca	Baños del Inca	La mesma	784674	9220370	Deposit
21	Cajamarca	Celendín	José Galvez	Cerro Lázaro	810624	9233327	Deposit
22	Cajamarca	Chota	Huambos	Pululo	718968	9286276	Deposit
23	Cajamarca	San Marcos	Ichocan	Llanupacha	820181	9184347	Quarry
24	Cajamarca	Santa Cruz	Santa Cruz	Piedra Blanca	726237	9267049	Quarry
25	Cusco	Canchis	San Pedro	Auquisa Dos	245689	8432456	Deposit
26	Cusco	Chumbivilcas	Llusco	Llusco I	809113	8413826	Quarry
27	Cusco	Chumbivilcas	Llusco	Llusco II	809848	8414374	Quarry
28	Cusco	Chumbivilcas	Santo Tomás	Santo Tomás I	813998	8401356	Quarry
29	Cusco	Chumbivilcas	Santo Tomás	Santo Tomás II	815350	8402623	Quarry
30	Moquegua	Mariscal Nieto	Moquegua	El Calicanto I	298927	8092960	Deposit
31	Moquegua	Mariscal Nieto	Moquegua	KAGIBEDA V	297325	8092367	Deposit
32	Moquegua	Mariscal Nieto	Moquegua	San Diego 5	295596	8091797	Deposit
33	Piura	Huancabamba	Sondorillo	Cascapampa	664564	9411821	Deposit

Table 1. *Cont.*

Code	Region	Province	District	Name	UTM Coordinates		Category
					East	North	
34	Puno	Carabaya	Corani	Cerro Huillacota	332446	8461578	Deposit
35	Puno	Carabaya	Corani	Cerro Huillacota	332877	8461280	Quarry
36	Puno	Carabaya	Macusani	Chillicuno	339363	8458070	Quarry
37	Puno	Chucuito	Juli	Cruzpata	453648	8207043	Quarry
38	Puno	Lampa	Palca	Umpuco	335360	8310123	Quarry
39	Puno	Lampa	Pucará	Cerro Llallahua	35.6062	8331301	Quarry
40	Puno	Melgar	Ayaviri	Cacapunco	324817	8342147	Quarry
41	Puno	San Antonio de Putina	Putina	Moroccarca	421765	8395996	Quarry
42	Tacna	Candarave	Quilahuani	Buena Vista	371012	8081711	Deposit
43	Tacna	Tacna	Tacna	Hospicio	361251	7990188	Deposit

However, Arequipa is the second most populated city in Peru, and in recent years, it has achieved accelerated population growth, without considering an urban plan, leading to the settlement of 25% of the million inhabitants in areas of moderate danger due to its proximity to the Misti and Chachani volcanoes. The historic center of Arequipa is built with ignimbrite, which gives the city an architectural peculiarity. With the purpose of promoting spaces with geological interest that become tools for education, dissemination, and communication of the dangers related to volcanic activity, INGEMMET proposed six pilot geosites near the city: (1) the ignimbrite quarries, where there is ignimbrite in the Arequipa Airport area; (2) Chili River Valley; (3) Misti and Chachani Volcanoes Viewpoint; (4) Nicholson Monogenetic Volcano; (5) Yura Monogenetic Field; and (6) Volcancillo Dome [4,5].

The material used in this work was collected in the quarries of Añashuayco and is limited to the area of accumulation of ignimbrite waste derived from the artisanal and informal exploitation of ignimbrite.

The OPC is the second most consumed product on Earth after water, with an annual global consumption during 2018 of around 4100 Mtons [6]. OPC is also the second largest source of anthropogenic carbon dioxide (CO_2) emissions, after power generation. Therefore, total emissions from the cement industry could contribute up to 8% of global CO_2 emissions [7]. Because of that, an environmentally friendly alternative to OPC consumption is necessary to reduce the high carbon dioxide consumption and improve green cement production. In recent years, geopolymers have attracted considerable attention among these binders due to their early compressive strength, low permeability, good chemical resistance, and excellent fire resistance behavior [8–11]. Geopolymers, which can be used as a green substitute for OPC, can be synthesized using different industrial and agricultural wastes [12,13] or natural pozzolan [10].

Geopolymerization process consists of the reaction of a solid aluminosilicate with a highly concentrated aqueous alkali hydroxide or silicate solution producing a synthetic alkali aluminosilicate material generically called a geopolymer [8,11,12], and results in amorphous or sub-crystalline spatial structures, similar to zeolites [14]. The structure of geopolymers consists of a polymeric Si-O-Al framework from chains of [SiO_4] and [AlO_4] tetrahedra with oxygen, shared corners forming a 3D network, and metal cations stabilizing the structure [8,9,14]. The metal cations most commonly used are sodium or potassium, and it is also possible to use calcium or lithium. Control of the alkaline solution that provides the metal cations is important in the geopolymerization process, NaOH being one of the most used possibilities [15]. A common example of the use of NaOH to activate the process

is the use of fly ash [16–18]. In the same way, in this work, NaOH was used as an alkaline solution for the production of geopolymers.

The high demand for housing and infrastructure has resulted in the generation of a substantial volume of waste as a result of increased construction activities. This is causing critical environmental and ecological problems for future generations, since construction and demolition waste is responsible for 30% of global solid waste [19,20]. Annually, the construction and ceramics industries generate billions of tons of construction demolition waste worldwide, including red clay bricks, ceramic tiles, and concrete waste; China alone contributes more than 2.3 billion tons, followed by the European Union and the United States with 800 and 700 million tons, respectively [21].

The use of waste material in the development of geopolymers can significantly contribute to a reduction in CO_2 footprint when these materials are compared to cement, concrete, or ceramic [22]. One possibility of great potential is the application of construction waste [23–25] or calcined clays [26] to implement geopolymers. In this work, geopolymer binders and mortars were developed from bricks, demolition mortars, and ignimbrite. A recent work has evaluated the use of ignimbrite powder in reactive powder concrete road pavement, showing the many possibilities of this material for construction [27]. Ignimbrite, as well as other pyroclastic vitreous volcanic rocks extracted directly from mining prospects, was previously studied for the realization of geopolymeric materials [28]. To our knowledge, there is no literature that studies the properties of geopolymers prepared from ignimbrite rocks from the Arequipa region in Peru.

The study of the mechanical properties of the most used geopolymeric materials obtained with the described processes has also been extensively analyzed in the literature [10,29–35]. Multiple works have been carried out studying the mechanical properties of geopolymeric cements reinforced with steel or different fibers [36–40], with different industrial wastes [41–43], or from construction demolition waste [24,25]. The aforementioned works give a broad idea of the many possibilities that geopolymeric materials have, and of the growing interest in the study of their mechanical properties. In this work, the mechanical properties of geopolymeric materials developed from demolition waste from the construction industry in Peru were analyzed.

Therefore, this work sought to reuse ignimbrite waste, calcined clay from demolition bricks, and demolition mortar from the construction industry in Arequipa for the manufacture of a novel geopolymeric binder material, which has properties, characteristics, and applications similar to those of ordinary Portland cement (OPC). The main novelty of this work is a deep characterization that has not been previously carried out of ignimbrite rock as well as a geological description of the ignimbrite rock from the region of Arequipa, Peru, and its use for the manufacture of high-quality geopolymer material for construction. There are no similar works that present methodologies or protocols for the use of ignimbrite rock waste. In this work, a novel methodology is proposed, based on the authors' research experience with other types of inorganic waste. The impact of advancing the study of geopolymers based on ignimbrite residues has value for all places (not just Peru) where this type of rock exists (volcanic zones).

The results of our work have been compared with conventional Portland cement mortars in order to analyze the mechanical, structural, and physical properties of the geopolymers obtained. It should be noted that this study shows a higher maximum resistance to uniaxial compression and modulus of elasticity of geopolymeric mortars with respect to Portland cement mortar prepared under the same conditions. The authors consider that this study offers interesting perspectives for the recycling of construction waste, and results that allow for understanding the behavior of the use of bricks, demolition mortars, and ignimbrite for the production of cement and geopolymeric mortars.

2. Material and Methods

2.1. Raw Materials and Characterization Techniques

The average chemical composition of ignimbrite rock is similar to rhyolite, it has a high content of silica and alumina, and traces of strontium, lithium, and rubidium have also been identified (Table 2). There are different types of ignimbrite rock [1], highlighting those that are white (compact and loose) and pink (compact and loose). Compact white ignimbrite has a massive, porous, permeable, and erosion-resistant appearance, generally with fragments of quartz, potassium feldspar, sheets of muscovite or biotite, and fragments of pumice constituting a heterogeneous aggregate, but with a uniform appearance. Microscopically, it generally contains plagioclase, sanidine or microcline, quartz, phyllosilicates such as muscovite or biotite depending on the chemical composition, and glass chips. Loose white ignimbrite is similar to white tuff but is less consolidated and less resistant to erosion. Its color is due to the greater presence of potassium feldspars, such as sanidine and orthose. On the other hand, pink ignimbrite has a chemical composition similar to that of white ignimbrite (Table 2). The reddish hue is obtained from hematite.

Table 2. Comparative table of the chemical composition of white and pink ignimbrite rock by XRF analysis (in wt %) [1].

	White Ignimbrite (wt %)	Pink Ignimbrite (wt %)
SiO_2	73.60	75.50
Al_2O_3	13.60	13.50
K_2O	4.23	4.64
Na_2O	3.94	3.44
Fe_2O_3	1.41	1.60
CaO	1.20	1.14
TiO_2	0.24	-
MgO	0.20	0.21
MnO	0.06	0.09
SO_3	0.06	0.04
P_2O_5	0.05	0.05
ZrO_2	0.04	0.04
SrO	0.03	0.04

The ignimbrite rock without any transformation was analyzed by X-ray microtomography (CT) to study its internal morphology. The size of the piece analyzed was a cube with dimensions 1 cm × 1 cm × 1 cm. Three types of raw materials were studied as potential sources of aluminosilicates that allow for the acquisition of new geopolymeric binders. The three raw materials used are currently considered inorganic waste from the construction industry in Arequipa (Peru), and they are calcined clay powder from demolition bricks (CCP), demolition mortar powder (DMP), and ignimbrite rock powder (IRP) [2,3], where CCP and DMP waste were obtained directly from demolished buildings in the city of Arequipa. Additionally, to obtain geopolymeric mortars, controlled additions of fine sand (FS) were considered, and for the geopolymerization process, addition of alkaline solutions of NaOH. For the preparation of the solutions, NaOH pellets (Biochem, Lima, Peru, 99% purity) and distilled water are added in adequate amounts for the required concentration, heating for 5 min with stirring at 80 °C. The solution is then expected to reach room temperature and mix with the dry raw materials. For the preparation of the solution, it is not an essential requirement to include the heating stage; the process can be carried out by means of a longer preparation time of the solution and constant stirring. The goal is to have a more homogeneous solution before mixing.

The starting materials were characterized physically, structurally, and microstructurally. Physical characterization was carried out by helium pycnometry (Quantachrome, model Pentapycnometer 5200e, Graz, Austria) and granulometry of laser light diffraction (Malvern Instruments, model Mastersizer 2000, Malvern, UK), determining the real density and average particle size, respectively. The materials were sieved by mesh size of 106 μm (ASTM sieve no. 140, Gilson, Columbus, USA). Micrographs of the samples were obtained using a Zeiss scanning electron microscope, model ZEISS MA LS 10 (Oberkochen, Germany).

X-ray microtomography is a non-destructive 3D imaging technique; it was applied to the ignimbrite rock to visualize properties related to the porosity and internal composition of the material. The equipment used for the measurement was an Xradia 610 Versa (Zeiss, Oberkochen, Germany). Measuring conditions: optical magnification = 0.4×, pixel size = 18.81 μm, current = 90 mA, voltage = 50 kV, images taken = 1018, image height = 1024, image width = 1004. The 3D images of the samples were rendered using the Fiji image processing package to visualize tomography-derived datasets. The porosity calculation was performed with AVIZO 9.4.0 software (Thermo Fisher Scientific, Waltham, USA). A crystallographic structural analysis of raw materials was performed by X-ray diffraction (XRD) using a D8 Focus diffractometer (Bruker, Karlsruhe, Germany) with a Cu tube (λ = 1.5406 Å), in the 2θ range of 5 to 100 and a step of 0.02. The present crystalline phases were identified using Diffrac.EVA 5.2 software (Bruker, Karlsruhe, Germany) and their Rietveld quantification was performed using Topas 6 software [44,45] for each type of raw material. Rietveld refinements were made using the fundamental parameter method. Some features such as zero error (2θ), sample displacement, and absorption and lattice parameters were treated as adjustable parameters to achieve the best fitting. The background was fitted by a fourth-order Chebyshev polynomial. For measurement configuration, we used the Lorentz polarization geometric factors. The robustness of the data obtained was corroborated from the values of several fitting indicators, such as goodness-of-fit (GOF) and residual factors (Rwp and RBragg) [44]. A chemical quantification of the present elements was carried out by total reflection X-ray fluorescence (TXRF) (BRUKER, model S2-PICOFOX, Karlsruhe, Germany), with a Mo tube and measurement time of 2000 s.

2.2. Preparation of Geopolymer and OPC Mortar

The three types of raw materials and fine sand were ground and sieved separately by ASTM no. 140 mesh under identical conditions. Geopolymeric binders and mortars were prepared following the specific route of this work, according to the path recommended in previous research work [46–49]. In the first stage, geopolymeric binders were obtained by mixing raw material powder (CCP, DMP, IRP) and sodium hydroxide solution with molar concentrations between 5 and 15 molar and at a 2:1 volumetric ratio for raw material powder and alkaline solution, respectively. In this work, it was decided to use the alkaline solution/raw material ratio of 0.5, as this ratio is within the average used for added water for OPC mortars (with typically used values ranging from 0.4 to 0.6). This ratio was used as a standard in fabricated materials, both geopolymeric and OPC mortars. After the mechanical evaluation of the geopolymeric binders, it was possible to determine the optimal conditions for the molar concentration of the sodium hydroxide solution, and in a second stage, geopolymeric mortars were manufactured, adding a controlled amount of fine sand to the paste of the geopolymer binder. For the manufacture of geopolymeric mortars, the volumetric ratio of raw material, fine sand, and NaOH solution was 2.00:3.33:1.00, corresponding to a composition in the mixtures in kg/m^3 that is presented in Table 3. The molar concentrations used for the preparation of the alkaline solution were 12, 15, or 18 molar. In both the preparation of binders and mortars, powders and alkaline solution were mixed until a homogeneous paste was obtained and then they were pressed in a 20 mm diameter cylindrical mold. The cylinders were demolded and deposited in airtight bags, where they cured for 24 h; after this time, they were removed from the bags and placed in the environment for 28 days. In this way, geopolymeric mortar from calcined

clay (GM-CC), geopolymeric mortar from demolition mortar (GM-DM), and geopolymeric mortar from ignimbrite rock (GM-IR) were obtained. This preparation time for 28 days is in accordance with other works and allows for correct workability of the samples [19,24]. The manufacture of conventional OPC mortars (M-PC) was considered using the same volumetric fractions of fine sand and binder, the same amount of water added, and the same molding and setting parameters.

Table 3. Mixing proportions for geopolymeric mortars studied.

Component	GM-CC	GM-DM	GM-IR	M-PC
FS (kg/m^3)	1676.4	1654.4	1634.1	1791.7
Raw material (kg/m^3)	1005.9	992.7	980.4	1075.0
Alkaline NaOH solution (kg/m^3)	502.9	496.3	490.2	537.5

2.3. Structural, Microstructural, and Mechanic Characterization of Geopolymeric and OPC Mortar

The structural crystallographic characterization of the mortars was carried out on a D8 Advance diffractometer (Bruker, Karlsruhe, Germany) with a Cu tube (λ = 1.5406 Å), equipped with a Vantec position-sensitive detector. The diffractometer had radial Soller slits and 60 mm Göbel mirrors for CuKα radiation (λ = 0.15405 nm) with parallel geometry in the incident beam. The parallel beam configuration in incident radiation allows for precise study of the crystalline structures for superficially inhomogeneous samples. Due to this characteristic, it was possible to directly mount and measure mortar specimens without grinding them. The tests were performed in the 2θ range from 5 to 90 and a step of 0.02. Identification of the crystalline phases and percentage of the amorphous phase was determined using Diffrac.EVA 5.2 software (Bruker, Karlsruhe, Germany). Due to the high presence of amorphous material in the solid specimens analyzed, a quantitative analysis of the crystalline phases was not carried out using the Rietveld method. The microstructural characterization was carried out on the same scanning electron microscopy equipment used for characterizing the starting raw materials. For microstructural studies, the samples were previously polished with lubricating liquid and diamond paste of particle size of 6 to 0.25 μm.

Mechanical evaluation was carried out in uniaxial compression tests (MICROTEST, model EM1/FR, Madrid, Spain) at a constant compression rate of 0.05 mm/min (Figure 3a). The samples used were 5 mm × 5 mm × 10 mm parallelepipeds, cut from larger cylindrical samples. Three repetitions were carried out for each sample (initial pieces in Figure 3b and tested samples with fragile behavior in Figure 3c). All mechanical tests were represented in stress versus strain curves and the maximum strength and modulus of elasticity could be determined. The data obtained for geopolymeric mortars were contrasted with those obtained on samples of conventional Portland cement mortars of similar geometry and dimensions.

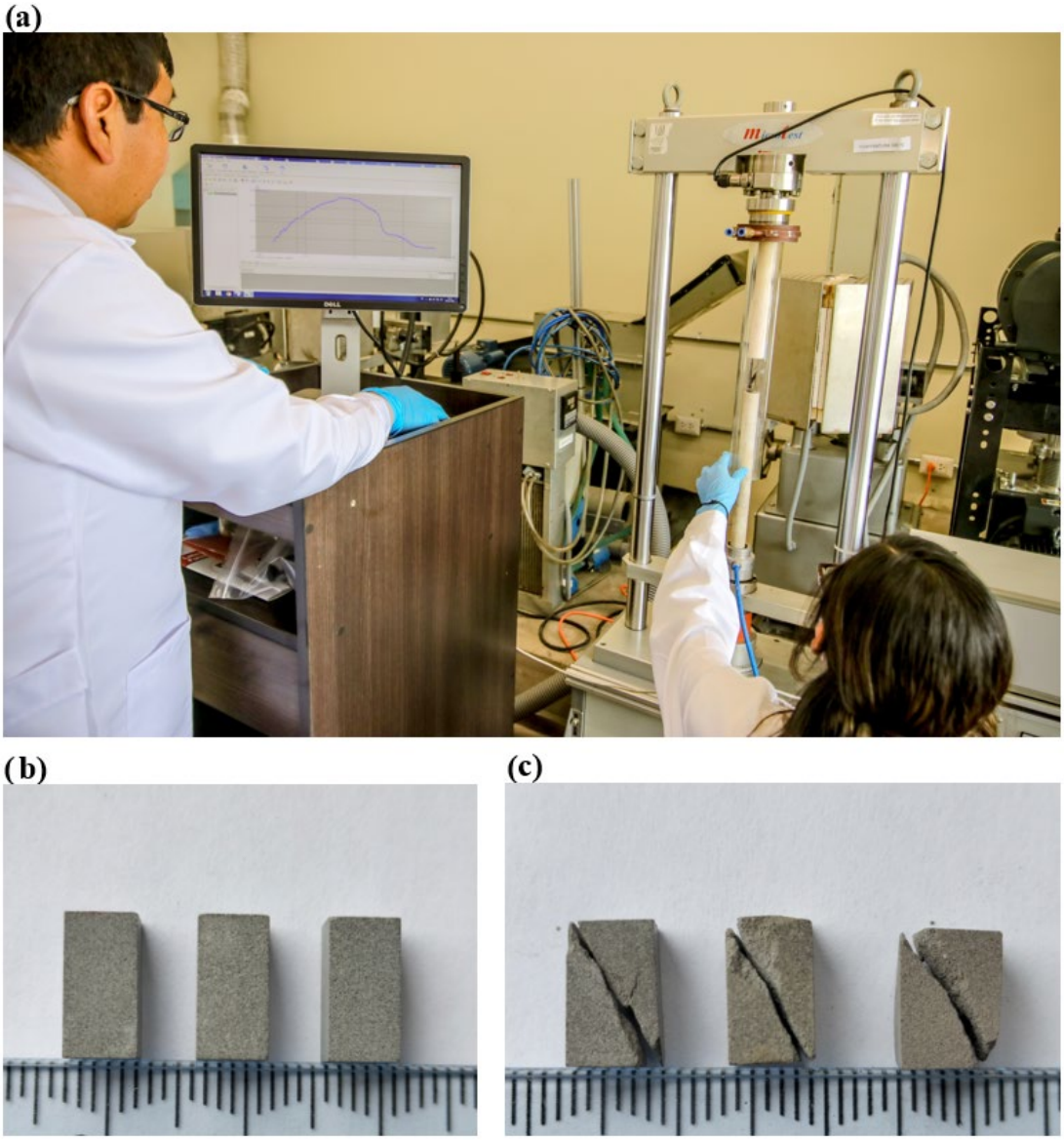

Figure 3. (**a**) Uniaxial compression test system. (**b**) Initial samples and (**c**) tested samples with fragile behavior, scale in the image of 1 mm between two attached lines.

3. Results and Discussion

3.1. Raw Materials

CT analysis was performed to understand the internal morphology and porosity of the ignimbrite rock. CT is a non-destructive technique for 2D or 3D sectional images based on the numerical reconstruction of the object from a series of projections [50]. The CT results with 2D and 3D representation are presented in Figure 4. The figure shows several 2D views where the different materials appear depending on their density. It can be observed that areas of materials with a lighter color come from higher elemental density, and other areas with a darker color come from areas with lower density chemical elements, where the darker areas, already practically black in color, come from the pores of the material.

A calculation of the porosity of the material was performed from the analysis of the CT images obtained for the total volume of the sample, obtaining a porosity of 0.97% by volume. It is a material with great construction abilities, with results comparable to those obtained in porosity calculation studies in cements with the same technique [51].

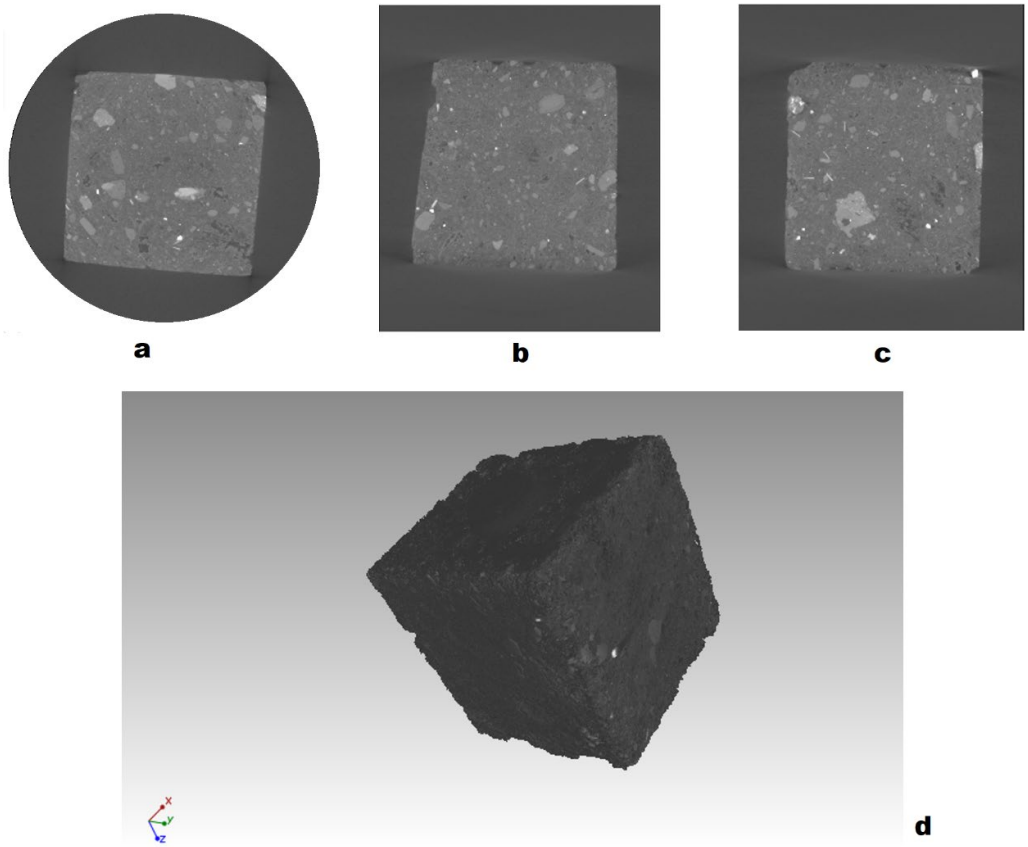

Figure 4. CT of the ignimbrite rock, with three different 2D views (**a**–**c**) and a 3D reconstruction of the 1 cm × 1 cm × 1 cm piece (**d**).

Table 4 shows the values found for the actual density of the starting powder materials, and in Figure 5, the average particle size distribution is presented. Actual density data were used to determine the mass quantities of the materials used to make mortars. On the other hand, for all materials, the values found for the average particle size range were between 70 and 84 µm. This result was expected since the materials were sieved using a mesh size of 106 µm. However, from the data in Figure 5, the presence of a minimum quantity of particles larger than 106 µm could be deduced, which can be explained by the presence of agglomerations other than what the particle size measurement equipment identified as larger particles. This can also be verified in Figure 6, where the scanning electron microscopy micrographs of the raw materials studied are shown, where the presence of agglomerated particles has been identified.

Table 5 shows the results obtained in the characterization by total reflection X-ray fluorescence. Given the characteristics of the technique, these values can be considered to be approximate values of the results obtained for major elements, and thus the values obtained serve to approximately establish the Si/Al ratios of the precursors and also to facilitate a correct search of the crystalline phases by XRD. Si/Al ratios of approximately 5:2, 4:1, 5:1, and 3:1 are observed for CCP, DMP, IRP, and FS, respectively. Taking into account the volume ratio of the mixtures of the materials with FS to make the mortars (2.00:3.33) and the previously measured density, a Si/Al ratio is obtained of approximately 6:2, 7:2, and 8:2 for the mortars obtained from DMP, IRP, and FS, respectively. The Si/Al ratios found can suggest the type of bond that forms in the new geopolymeric material; therefore, we can point out that the bonds formed must be of sialate type (Si/Al > 3) [9,48].

Table 4. Determination of the real density of the raw materials.

Raw Material	Weight (g)	Real Volume (cm^3)	Real Density (g/cm^3)
CCP	6.2478	2.3502	2.6584
DMP	6.3599	2.4802	2.5643
IRP	5.0702	2.0466	2.4774
FS	7.1178	2.6394	2.6967

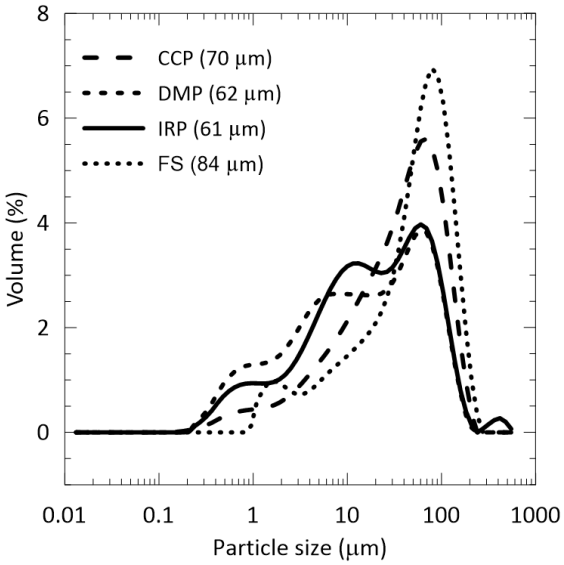

Figure 5. Particle size distribution of the raw materials.

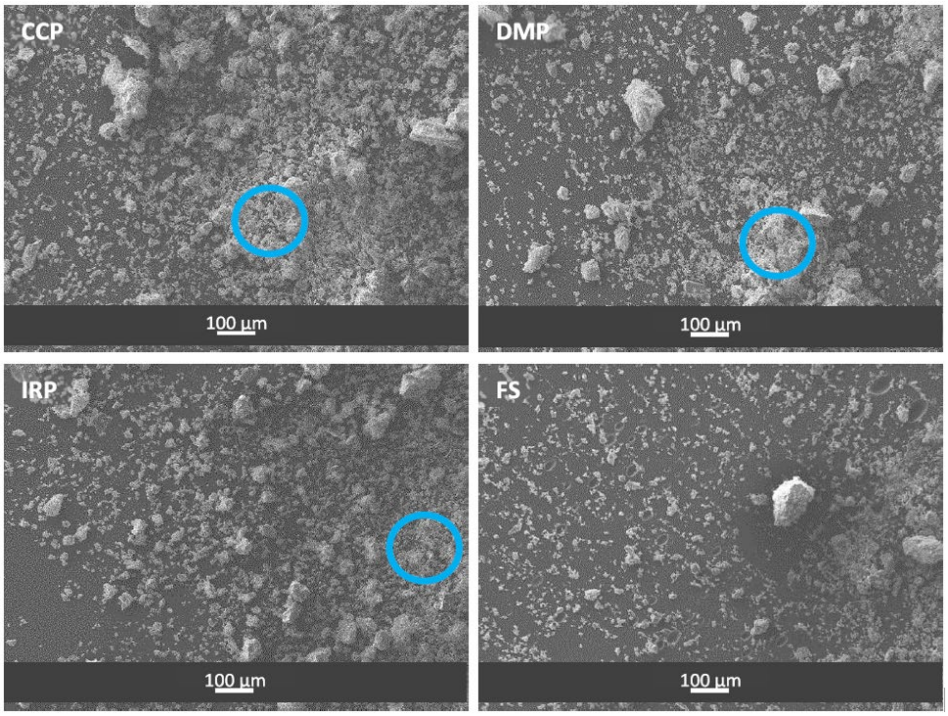

Figure 6. Scanning electron microscopy micrographs of the raw materials studied (CCP, DMP, IRP and FS). The presence of agglomerated particles (blue circles) was identified.

Table 5. Chemical characterization by total reflection X-ray fluorescence of the raw materials.

Elements	CCP	DMP	IRP	FS
	Si/Al~5:2	Si/Al~4:1	Si/Al~5:1	Si/Al~3:1
	mg/kg			
Al	30,180.00 ± 3604.26	16,363.00 ± 53.74	26,496.67 ± 1086.66	27,026.67 ± 1167.79
Si	78,093.33 ± 7583.89	68,435.00 ± 2156.68	136,373.33 ± 4622.92	90,120.00 ± 3592.51
P	357.90 ± 41.40	1059.80 ± 25.74	112.17 ± 16.67	479.13 ± 18.53
Cl	156.55 ± 5.44	331.25 ± 2.19	240.87 ± 31.26	374.27 ± 5.02
K	7197.33 ± 779.61	7175.00 ± 159.81	16,586.67 ± 1055.00	7958.00 ± 448.02
Ca	8329.67 ± 1195.03	98,380.00 ± 1781.91	4995.67 ± 131.20	19,018.00 ± 1325.10
Ti	1933.80 ± 315.46	1133.00 ± 32.81	921.15 ± 155.92	2172.90 ± 181.80
Cr	19.34 ± 1.98	14.38 ± 0.22	-	29.46 ± 4.22
Mn	437.80 ± 52.75	270.09 ± 5.39	359.80 ± 56.81	284.36 ± 25.06
Fe	24,631.67 ± 3325.44	16,697.00 ± 131.52	6056.25 ± 75.31	17,918.33 ± 1725.66
Ni	8.79 ± 1.52	7.61 ± 0.23	12.44 ± 3.28	9.93 ± 0.74
Cu	56.47 ± 9.34	49.70 ± 7.23	29.65 ± 0.03	28.08 ± 2.34
Zn	62.21 ± 7.24	46.89 ± 5.33	48.74 ± 1.83	41.09 ± 2.54
As	15.43 ± 1.51	7.61 ± 1.17	-	-
Rb	47.20 ± 7.00	25.16 ± 0.45	68.38 ± 9.25	27.91 ± 2.59
Sr	223.66 ± 45.51	242.66 ± 19.00	126.72 ± 13.39	445.65 ± 45.43
Ba	595.53 ± 80.33	358.50 ± 22.63	941.50 ± 70.63	577.30 ± 47.93
Pb	14.44 ± 2.23	10.37 ± 0.10	16.35 ± 1.88	13.80 ± 2.17
Br	-	1.42 ± 0.01	-	1.06 ± 0.05

Figure 7 shows the diffractograms obtained for CCP (Figure 7a), DMP (Figure 7b), IRP (Figure 7c), and FS (Figure 7d), where the main Bragg peaks of the detected phases are marked. The crystalline phases found are consistent with the results of TXRF. In the figures, a continuous line can be seen in the lower part of the diffractograms on which the peaks of the crystalline phases are located. The part of the diffractogram on said line would mark the crystalline part, while in the lower zone, it can be estimated that it is mainly the amorphous part [52]. It can be said that, in general, the samples are quite crystalline, given the great intensity of the peaks compared to the area under the curve. According to this qualitative interpretation, the FS sample would be the most crystalline by far, the IRP sample the next in the crystallinity level, followed by the CCP and DMP samples, with the latter being the least crystalline in the series. The results obtained by XRD and TXRF for IRP are consistent with the CT images obtained, depending on the density of the materials.

Table 6 shows the main phases identified and their Rietveld quantification. The presence of a high content of aluminosilicates is evident for the three types of raw materials, which could have led to a greater degree of geopolymerization [9,46,47]. It could be suggested that the sodium (albite), calcium (anorthite), and potassium (microcline) aluminosilicates are, to a large degree, responsible for the geopolymerization process of the crystalline fraction of CCP, DMP, and IRP, respectively. The mixture with FS to make mortars would also favor geopolymerization because of the high presence of anorthite in its composition.

Table 6. Identification and quantification of crystalline phases present in the raw materials.

Crystalline Phases	CCP	DMP	IRP	FS
	%Weight			
Quartz (SiO_2)	14	7.9	-	-
Albite ($NaAlSi_3O_8$)	40.5	10.8	22.3	10.9
Muscovite 2M1 ($KAl_3Si_3O_{10}(OH)_2$)	28.1	9	1.6	9.1
Cristobalite (SiO_2)	9.6	4.8	38.9	3.4
Actinolite ($Ca_2(Mg,Fe^{2+})_5Si_8O_{22}(OH)_2$)	6.2	3.5	-	5.1
Anatase (TiO_2)	1.6	-	-	-
Anorthite ($CaAl_2Si_2O_8$)	-	40.9	-	71.5
Portlandite ($Ca(OH)_2$)	-	8.5	-	-
Calcite ($Ca(CO)_3$)	-	10.6	-	-
Chlorite ($(Mg,Al)_6(Si,Al)_4O_{10}(OH)_8$)	-	4	-	-
Microcline ($KAlSi_3O_8$)	-	-	37.2	-

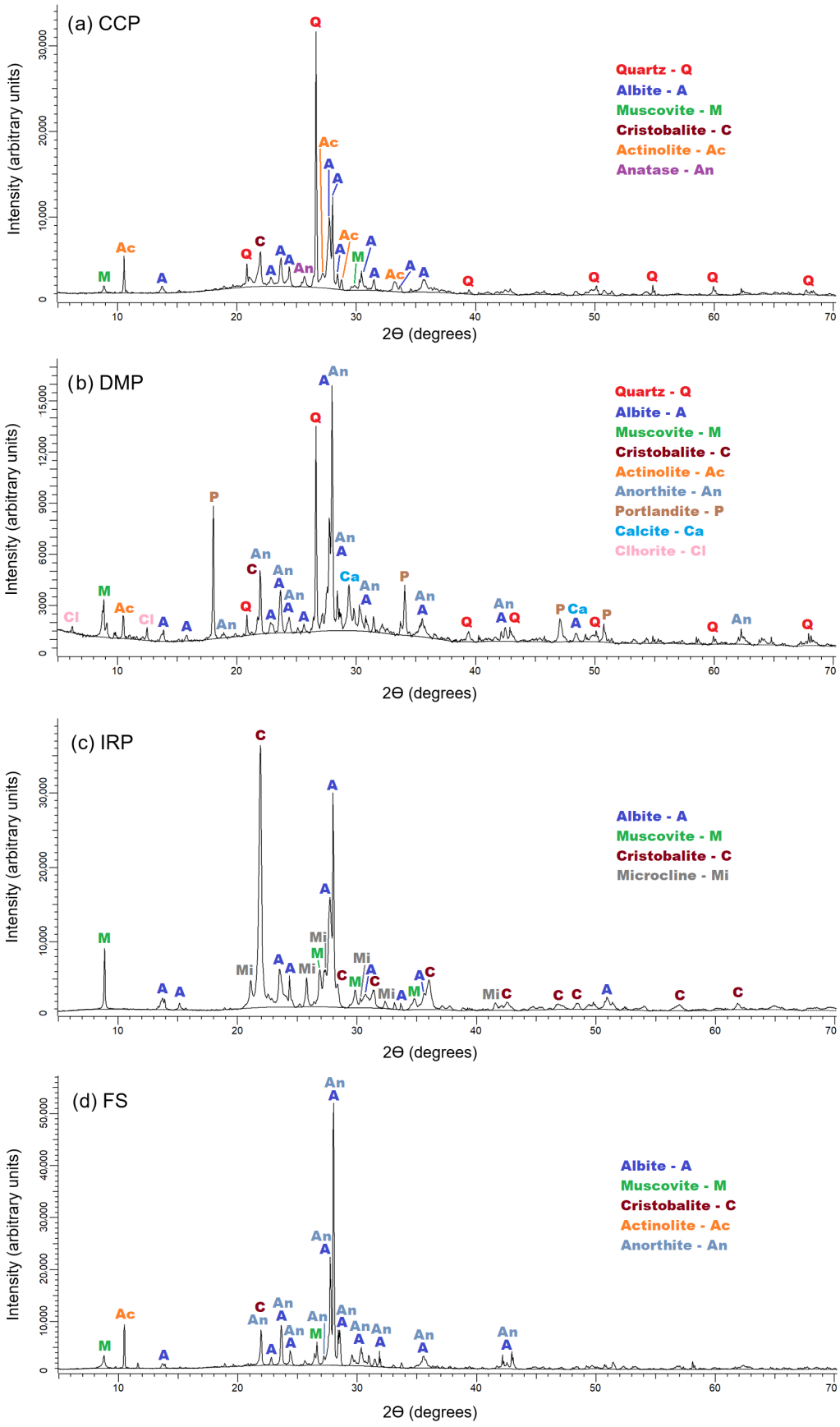

Figure 7. Diffractograms recorded for the raw materials with the main Bragg peaks of the present phases marked for (**a**) CCP, (**b**) DMP, (**c**) IRP, and (**d**) FS.

3.2. Geopolymeric and OPC Mortars

Figure 8 shows the diffractograms obtained where the main crystalline phases have been identified for GM-CC (Figure 8a), GM-DM (Figure 8b), GM-IR (Figure 8c), and M-PC (Figure 8d). In the figure, the main Bragg peaks of the detected phases are marked. The figure clearly shows how, in general, the amorphous part, which would be the lower part of the continuous curve in the area below the diffractogram [52], would be very high, compared to the raw materials (see Figure 7 and the qualitative explanation of the crystallinity grade for the raw materials). In this way, in general, all mortars are quite amorphous, being the most crystalline case, without reaching a very high degree compared to the raw materials, such as that of the GM-IR sample. This high degree of amorphousness of the mortars obtained is in line with the general characteristics of geopolymeric mortars [9,53]. On the other hand, Figure 9 shows a representation of bars of a semiquantitative estimate of the percentage of amorphous phase for each geopolymeric mortar studied and its comparison with the percentage of amorphous phase of OPC mortar, using Diffrac.EVA 5.2 software (Bruker, Germany) [52]. All studied mortars have a high degree of amorphous material coming from the geopolymer [9], GM-IR being the least amorphous.

The crystalline phases observed for each material are as follows:

Geopolymeric mortar from calcined clay (GM-CC): quartz (SiO_2), albite ($NaAlSi_3O_8$), and microcline ($KAlSi_3O_8$).
Geopolymeric mortar from demolition mortar (GM-DM): quartz (SiO_2) and anorthoclase ($(Na_{0.85}K_{0.15})AlSi_3O_8$).
Geopolymeric mortar from ignimbrite rock (GM-IR): quartz (SiO_2), albite ($NaAlSi_3O_8$) and sanidine (KSi_3AlO_8).
Mortar from Portland cement (M-PC): anorthoclase ($(Na_{0.85}K_{0.15})AlSi_3O_8$).

From the previous paragraph and considering the phases found in the raw materials, it could be suggested that Na from the initial albite and the incorporation of Na^+ ions in the aluminosilicate structures of the precursor materials have made possible the formation of new crystalline phases in the manufactured geopolymers. Thus, from the phases with the presence of K, the formation of microcline from muscovite, anorthoclase from anorthite with K contribution from muscovite, and sanidine from microcline can be suggested, for GM-CC, GM-DM, and GM-IR, respectively.

Figure 10 shows micrographs by scanning electron microscopy of polished surfaces of conventional geopolymeric and OPC mortars. For all the materials, it was possible to identify two phases very well differentiated from each other; on the one hand, a continuous phase of binder material and, on the other, a discontinuous phase of fine sand grains characterized by a typical morphology of equiaxiated grains immersed in the phase binder continues. From these images, it can be understood that the FS does not geopolymerize to a great extent, and the aluminosilicates that cause this process come mainly from raw materials.

Figure 11a shows the stress versus strain curves for the geopolymer binders after being cured for 28 days in air. This preparation time is in accordance with previous works and allows for correct workability of the samples [19,24]. It should be noted that the pastes obtained from the mixture of binder raw materials and alkaline solutions of 5 molar concentration did not have the cohesion and compactability necessary to obtain adequate samples and were discarded. On the other hand, the alkaline solution of 15 M produced a workable and moldable paste with good mechanical strength. To reduce the amount of alkaline compound without damaging mechanical resistance, 12 M and 18 M preparations were made for the geopolymeric mortar manufacturing stage. As will be seen in the particular study of the results, it was generally found that for concentrations 12 M and 15 M, there is no significant gain in mechanical resistance, but for 18 M, there is a decrease. Geopolymers with 18 M molarity had high plasticity, and their molding process was complex; however, it was possible to manufacture geopolymers satisfactorily. In general, the best overall results were obtained for the 12 M concentration.

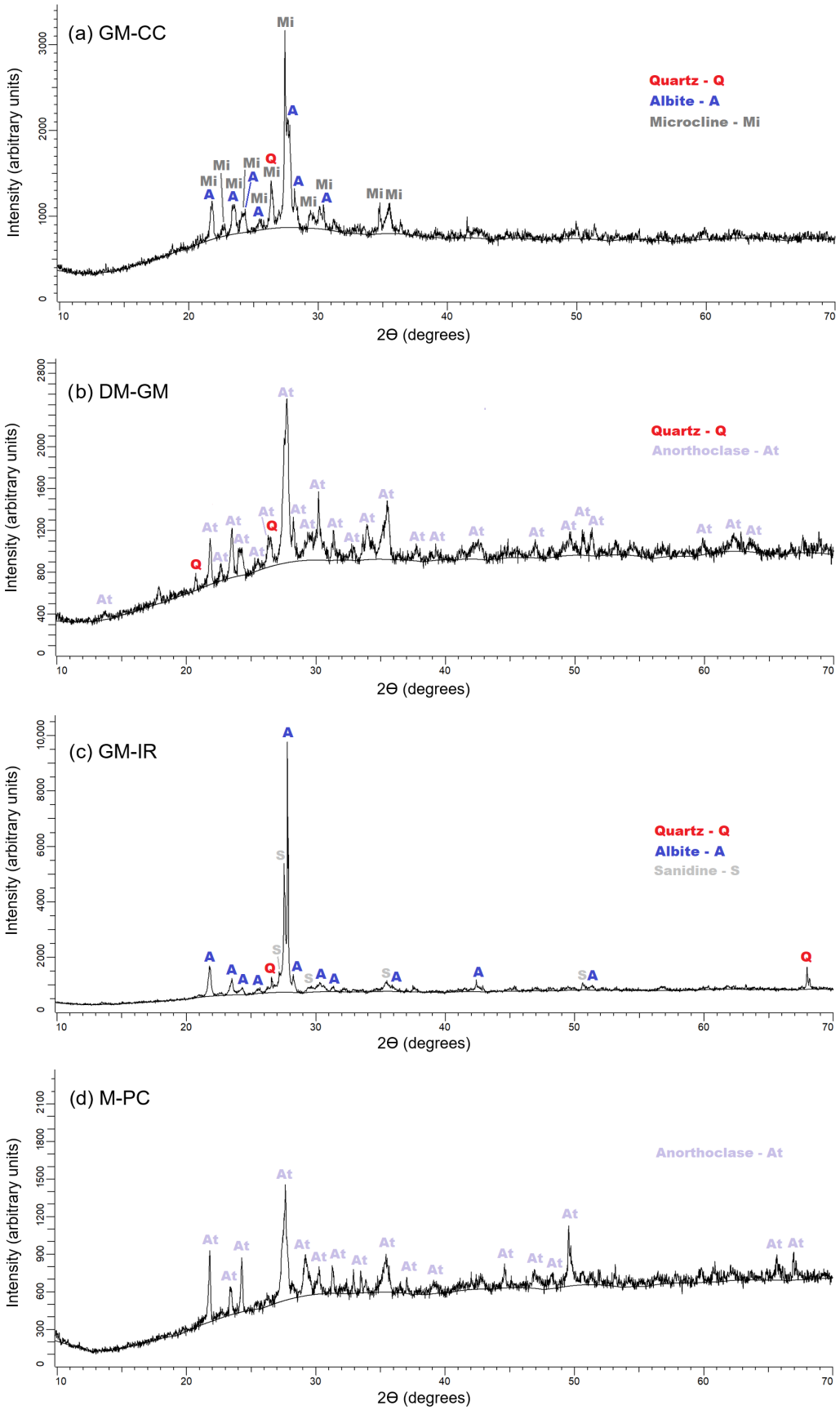

Figure 8. Diffractograms recorded for geopolymeric and OPC mortar with the main Bragg peaks of the present phases marked for (**a**) GM-CC, (**b**) GM-DM, (**c**) GM-IR, and (**d**) M-PC.

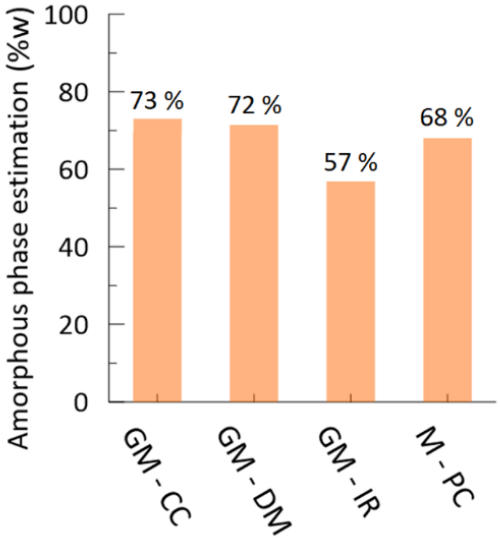

Figure 9. Comparison of a semiquantitative estimation of the percentage of amorphous phase of geopolymeric (GM-CC, GM-DM, and GM-IR) and conventional mortars of OPC (M-PC).

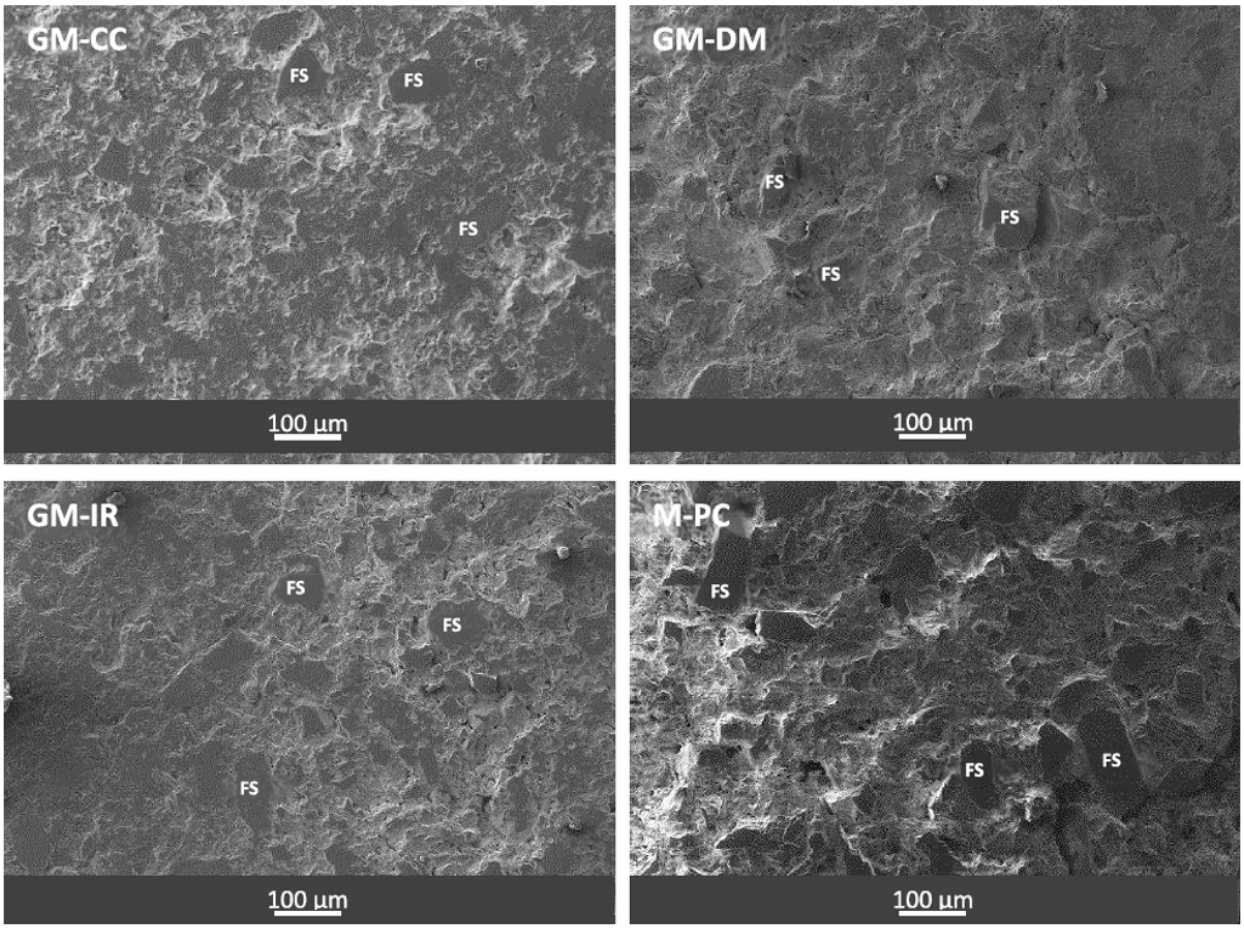

Figure 10. Scanning electron microscopy micrographs of geopolymeric mortars (GM-CC, GM-DM, GM-IR) and their comparison with conventional Portland cement concrete (M-PC) showing the situation of FS for all cases.

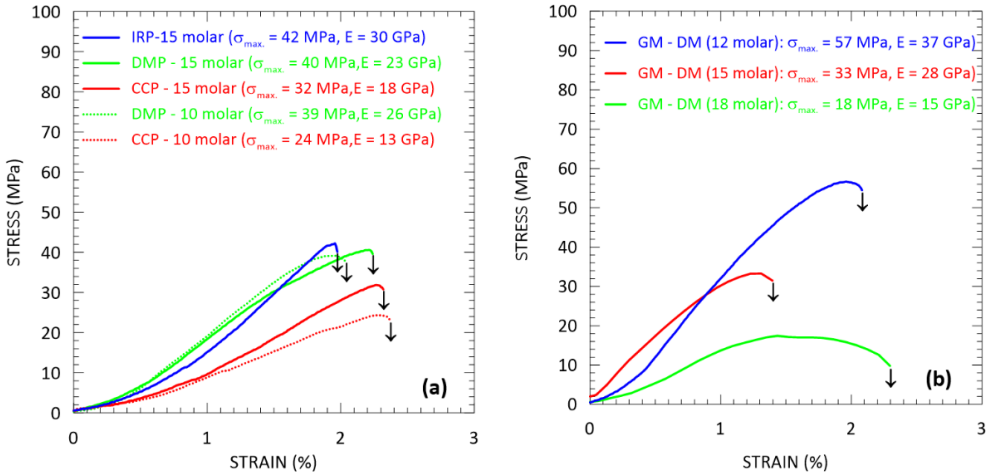

Figure 11. Stress versus strain curves for (**a**) IRP, CCP, and DMP geopolymer binders, and (**b**) DMP geopolymeric mortars with varied alkaline solution molarities.

From the curves of Figure 11a, higher values of maximum resistance to uniaxial compression and modulus of elasticity can be observed in binders derived from IRP, with respect to their DMP and CCP counterparts when obtained with alkaline molarity solutions of 15 M. Furthermore, reducing the molarity of the alkaline solution from 15 to 10 M produces a slight reduction in compressive strength, although it is more evident in CCP-derived binders, reducing its resistance from 32 to 24 MPa and its modulus of elasticity from 18 to 13 GPa. Comparing the results obtained with the influence of the chemical activation process by NaOH on the compressive stresses of geopolymers in previous works, the values obtained in this work are good and have similar molarity values [24,48].

In Figure 11b, a comparison of stress versus strain curves is made for DMP geopolymeric mortars with alkaline solution concentrations of 12, 15, and 18 M. The results reflect a systematic reduction in compressive strength when the concentration of the alkaline solution increases from 12 to 18 M. It is important to mention that the 18 M concentration is not recommended, according to the results of this work, since it reduces the overall resistance of the manufactured geopolymer. This reduction in mechanical resistance could be due to the accumulation and crystallization of secondary compounds (NaOH or other Na compounds) in the geopolymer binder interfaces and fine sand, which could produce an inadequate transmission of stress between both phases, an effect that is more significant with an excess concentration of sodium ions in the alkaline solution used.

It was demonstrated that ignimbrite rock powder as a binder material (without the addition of aggregates) presented the best mechanical characteristics, among the three types of binder raw materials used in this work, with values of compressive strength of 42 MPa and a modulus elastic of 30 GPa, when activated with a 15 M sodium hydroxide solution. The results show that the increase in the molar concentration of the sodium hydroxide hardening solution did not increase the compressive strength or the elastic modulus; on the contrary, it reduced it, finding that the best mechanical results were obtained when going from 18 to 12 molar; this result is systematic and reproducible for the three types of geopolymeric mortars studied.

Figure 12 shows stress versus strain curves for geopolymer mortars of calcined clay powder (GM-CC), demolition mortar powder (GM-DM), ignimbrite rock powder (GM-IR), and conventional Portland cement mortars (M-PC). All tests were carried out with four repetitions and under normal environmental conditions. The results in Figures 11 and 12 are presented in percentages, generally obtaining values of the order of 2%, which is equivalent to 0.02 deformation. In this work, the results were expressed in % to facilitate understanding of the graphs. The value close to 2% is consistent with other works in the literature and the expected values for mortars manufactured from Portland cement. When comparing the data obtained only for geopolymeric mortars, it can be mentioned that the highest values in

compressive strength and modulus of elasticity were for GM-CC, followed by GM-DM and GM-IR. The worst values obtained for GM-IR coincide with the higher crystallinity shown by XRD (Figure 9) that can be related to a lower geopolymerization of GM-IR compared to GM-CC and GM-DM [9,14]. The highest maximum resistance to uniaxial compression and modulus of elasticity of geopolymeric mortars is shown with respect to Portland cement mortar in the study conditions of this work. According to previous reports, the modulus of elasticity of geopolymer materials is generally lower than that of OPC materials, which is one of the significant weaknesses and disadvantages of geopolymer concretes. However, this does not happen in all cases, and in certain geopolymeric materials, similar or even better values are obtained than OPC-prepared mortars [48,49]. The mode of preparation of M-PC in this work is not the conventional way of preparation, so by preparing these mortars under more standardized conditions, we consider that their mechanical properties can be significantly improved. In any case, this work offers a perspective of the great potential of the geopolymeric materials studied.

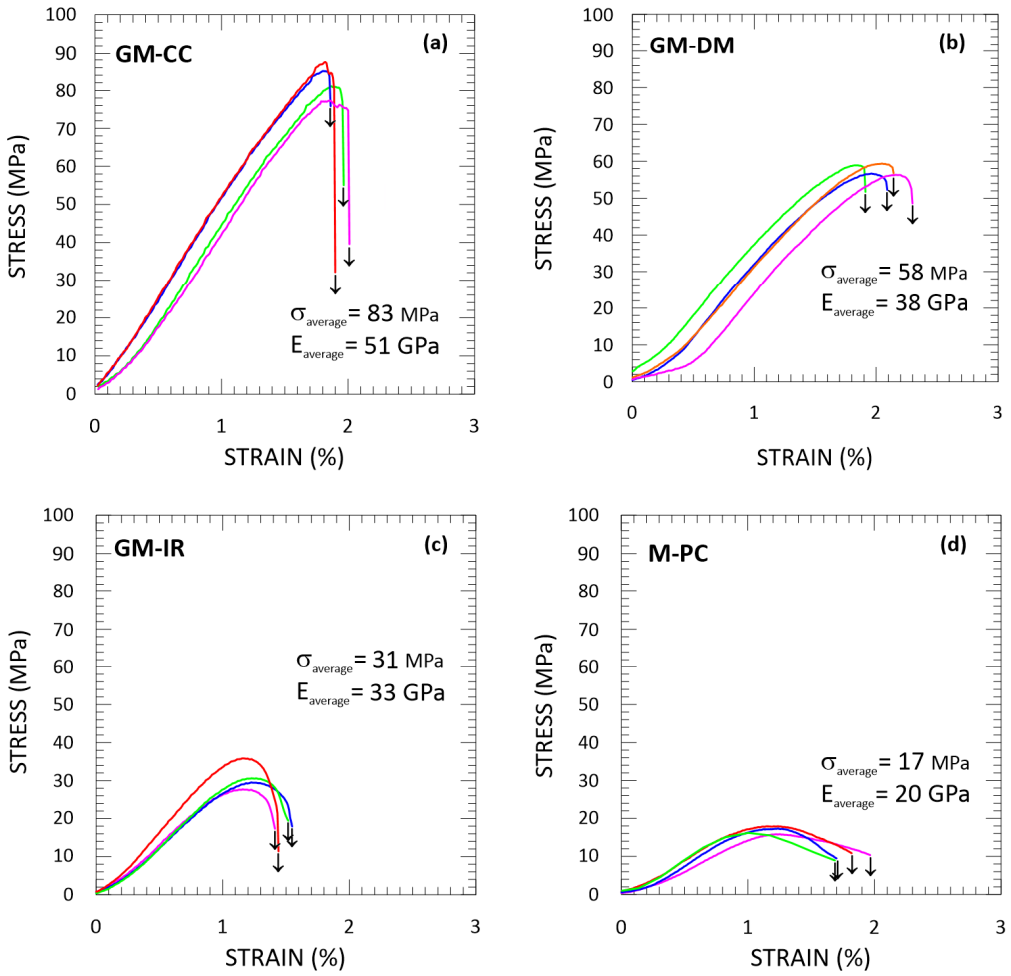

Figure 12. Stress versus strain curves for (**a**–**c**) conventional geopolymeric mortars and (**d**) Portland cement mortars, tested in air at room temperature for four repetitions in each case.

Figure 13 presents two comparative graphs in which all the mechanical data obtained in the uniaxial compression tests are summarized. These graphs show the degree of repetitiveness of the results, which is accompanied by the homogeneity of the samples. In general, values of the same order or relatively stable are obtained for both the uniaxial compressive strength and the modulus of elasticity. The elastic modulus was calculated directly from the stress versus strain curves; it is the result of measuring the slope in the linear elastic zone of each of the curves in Figure 12 for mortars. A greater repetitiveness can be seen,

with respect to the compressive strength values (Figure 13a), of the results in geopolymeric DMP mortars and OPC mortars. However, observing Figure 13b, a greater repetitiveness of the results of the modulus of elasticity can be seen in the geopolymeric mortars of CCP and DMP, with respect to the geopolymeric mortars of IRP and the conventional mortars of OPC.

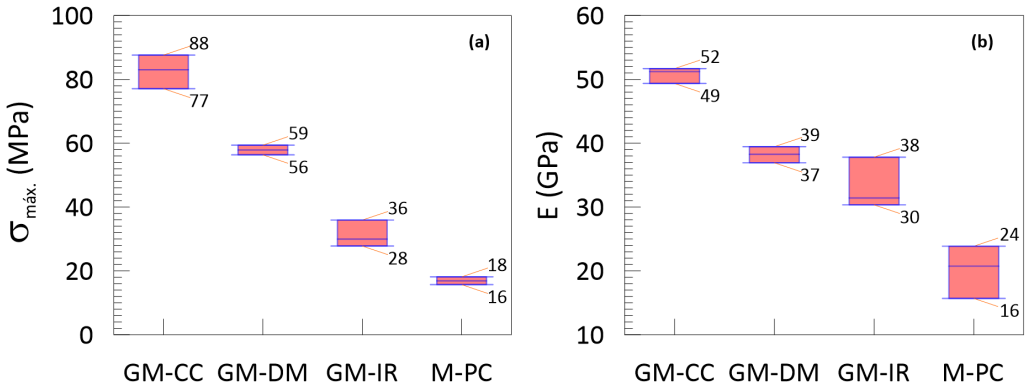

Figure 13. Comparative summary of values of (**a**) maximum resistance to uniaxial compression and (**b**) modulus of elasticity, for conventional and geopolymeric Portland cement mortars.

This study demonstrated that it is possible to obtain geopolymeric mortars without the addition of Portland cement, with maximum compressive strength values and elastic moduli higher than those of conventional Portland cement mortars. The best results were found for calcined clay powder mortars, followed by demolition mortar powder mortars and followed by ignimbrite rock powder mortars, this last type of mortar is of particular relevance due to the potential use of ignimbrite waste for the manufacture of new construction materials, considering that currently, this waste only accumulates in the quarries where it is exploited, and there are no similar studies that provide insights or recommendations for its use.

4. Conclusions

A deep characterization and geological description of ignimbrite rock from the region of Arequipa, Peru was carried out in this work. An ignimbrite rock was characterized, obtaining a porosity by CT technique of 0.97% by volume, verifying the known constructive capacity of this geological material.

In this work, ecofriendly geopolymeric binders and mortars, without the addition of ordinary Portland cement, were successfully manufactured from inorganic waste from the construction industry: ignimbrite rock powder, calcined clay powder, and demolition mortar powder. Aluminosilicates of sodium (albite), calcium (anorthite), and potassium (microcline) were found in high percentages, by XRD, in the starting powders of calcined clay, demolition mortar, and ignimbrite rock, respectively, suggesting that these phases would be responsible for the geopolymerization process (in the crystalline region) to obtain geopolymer binders and mortars. The Si/Al ratios found in all starting powders suggest that the bonds formed in the geopolymeric materials studied are sialate (Si/Al > 3).

Na from initial albite and the incorporation of Na^+ ions in the aluminosilicate structure of the precursor materials enables the formation of new crystalline phases in the prepared geopolymers. The formation of microcline from muscovite, anorthoclase from anorthite with K contribution from muscovite, and sanidine from microcline are suggested for calcined clay geopolymeric mortars, geopolymeric demolition mortar, and ignimbrite rock geopolymeric mortar, respectively. For conventional and geopolymeric Portland cement mortars, it was possible to identify by scanning electron microscopy two very well-differentiated phases: on the one hand, a continuous phase of the binder material, and on the other, a discontinuous phase of fine sand grains immersed in the continuous binder phase.

Higher values of maximum resistance to uniaxial compression and modulus of elasticity can be observed in binders derived from IRP compared to CCP and DMP, obtained with 15 M alkaline molarity solutions. Furthermore, reducing the molarity of the alkaline solution from 15 to 10 M produces a reduction in the compressive strength for all geopolymeric binders. The highest values in the compressive strength and modulus of elasticity for mortars were for GM-CC, followed by GM-DM and GM-IR. It was found that the values of maximum resistance to uniaxial compression and modulus of elasticity are systematically higher in geopolymeric mortars from the construction industry compared to Portland cement, preparing mortars under the conditions of this work.

In this study, characterization of the ignimbrite of the Arequipa, Peru region was carried out. This work demonstrates the enormous potential of the construction waste studied, namely, the raw material of alternative mortar binders without the addition of OPC. Ignimbrite generally shows good results as a geopolymeric precursor. As a conclusion, in general, the best overall results were obtained for the 12 M concentration for all the materials, and the optimal values were obtained in maximum resistance to uniaxial compression and modulus of elasticity for 15 M alkaline solutions of ignimbrite without the addition of aggregates, with values of compressive strength of 42 MPa and a modulus elastic of 30 GPa.

Further research is needed on the long-term technical performance, durability, and economic feasibility of geopolymeric building products made from recycled inorganic waste from the construction industry.

Author Contributions: Conceptualization, F.A.H.-M. and S.M.-C.; methodology, F.A.H.-M. and S.M.-C.; software, F.A.H.-M., C.K.P.-Ñ. and S.M.-C.; validation, F.A.H.-M. and S.M.-C.; formal analysis, F.A.H.-M., C.K.P.-Ñ., M.d.M.O.C. and S.M.-C.; investigation, F.A.H.-M., C.K.P.-Ñ., M.d.M.O.C. and S.M.-C.; resources, F.A.H.-M., M.d.M.O.C. and S.M.-C.; data curation, F.A.H.-M. and S.M.-C.; writing—original draft preparation, F.A.H.-M. and S.M.-C.; writing—review and editing, F.A.H.-M., C.K.P.-Ñ., M.d.M.O.C. and S.M.-C.; visualization, F.A.H.-M. and S.M.-C.; supervision, F.A.H.-M.; project administration, F.A.H.-M.; funding acquisition, F.A.H.-M. and M.d.M.O.C. All authors have read and agreed to the published version of the manuscript.

Funding: This study was funded by Consejo Nacional de Ciencia, Tecnología e Innovación Tecnológica (CONCYTEC) and Servicio Nacional de Capacitación para la Industria de la Construcción (SENCICO) from Peru (grant number 106-2017-FONDECYT). University of Seville through the VII Plan Propio de Investigación (Proyect 2022/00000279).

Data Availability Statement: All data are included in this article.

Acknowledgments: CONCYTEC and SENCICO from Peru and the University of Seville through the VII Plan Propio de Investigación. The authors are grateful to the X-ray Laboratory and Functional Characterization Services of the Centro de Investigación Tecnología e Innovación de la Universidad de Sevilla (CITIUS).

Conflicts of Interest: The authors declare no conflicts of interest.

References

1. Díaz, A.; Manrique, S.; Siancas, L. Compendio de Rocas Ornamentales En El Perú. *INGEMMET Bol. Ser. B Geol. Econ.* **2020**, *70*, 1–286.
2. Lebti, P.P.; Thouret, J.C.; Wörner, G.; Fornari, M. Neogene and Quaternary Ignimbrites in the Area of Arequipa, Southern Peru: Stratigraphical and Petrological Correlations. *J. Volcanol. Geotherm. Res.* **2006**, *154*, 251–275. [CrossRef]
3. Brandmeier, M.; Wörner, G. Compositional Variations of Ignimbrite Magmas in the Central Andes over the Past 26 Ma—A Multivariate Statistical Perspective. *Lithos* **2016**, *262*, 713–728. [CrossRef]
4. Aguilar, R.; Thouret, J.C.; Samaniego, P.; Wörner, G.; Jicha, B.; Paquette, J.L.; Suaña, E.; Finizola, A. Growth and Evolution of Long-Lived, Large Volcanic Clusters in the Central Andes: The Chachani Volcano Cluster, Southern Peru. *J. Volcanol. Geotherm. Res.* **2022**, *426*, 107539. [CrossRef]
5. Manrique Llerena, N.; Arias Salazar, C.; de Vries, B.; Aguilar Contreras, R.; Palacios, C. Ruta Del Sillar: Quebrada de Añashuayco, Arequipa-Perú. *Libr. Resúm. IX Foro Int. Peligros Volcánicos-IX FIPVO* **2023**, *3*, 389–393.
6. U.S. Geological Survey. *Mineral Commodity Summaries 2019*; Tolcin, A.C., Ed.; USGS: Reston, VA, USA, 2019. [CrossRef]
7. Andrew, R.M. Global CO_2 Emissions from Cement Production, 1928–2017. *Earth Syst. Sci. Data* **2018**, *10*, 2213–2239. [CrossRef]

8. Duxson, P.; Fernández-Jiménez, A.; Provis, J.L.; Lukey, G.C.; Palomo, A.; Van Deventer, J.S.J. Geopolymer Technology: The Current State of the Art. *J. Mater. Sci.* **2007**, *42*, 2917–2933. [CrossRef]
9. Davidovits, J. Geopolymers: Ceramic-like Inorganic Polymers. *J. Ceram. Sci. Technol.* **2017**, *8*, 335–350. [CrossRef]
10. Firdous, R.; Stephan, D.; Djobo, J.N.Y. Natural Pozzolan Based Geopolymers: A Review on Mechanical, Microstructural and Durability Characteristics. *Constr. Build. Mater.* **2018**, *190*, 1251–1263. [CrossRef]
11. Ma, C.K.; Awang, A.Z.; Omar, W. Structural and Material Performance of Geopolymer Concrete: A Review. *Constr. Build. Mater.* **2018**, *186*, 90–102. [CrossRef]
12. Asim, N.; Alghoul, M.; Mohammad, M.; Amin, M.H.; Akhtaruzzaman, M.; Amin, N.; Sopian, K. Emerging Sustainable Solutions for Depollution: Geopolymers. *Constr. Build. Mater.* **2019**, *199*, 540–548. [CrossRef]
13. Emdadi, Z.; Asim, N.; Amin, M.H.; Yarmo, M.A.; Maleki, A.; Azizi, M.; Sopian, K. Development of Green Geopolymer Using Agricultural and Industrialwaste Materials with High Water Absorbency. *Appl. Sci.* **2017**, *7*, 514. [CrossRef]
14. Koleżyński, A.; Król, M.; Żychowicz, M. The Structure of Geopolymers—Theoretical Studies. *J. Mol. Struct.* **2018**, *1163*, 465–471. [CrossRef]
15. Arnoult, M.; Perronnet, M.; Autef, A.; Rossignol, S. How to Control the Geopolymer Setting Time with the Alkaline Silicate Solution. *J. Non. Cryst. Solids* **2018**, *495*, 59–66. [CrossRef]
16. Hanjitsuwan, S.; Hunpratub, S.; Thongbai, P.; Maensiri, S.; Sata, V.; Chindaprasirt, P. Effects of NaOH Concentrations on Physical and Electrical Properties of High Calcium Fly Ash Geopolymer Paste. *Cem. Concr. Compos.* **2014**, *45*, 9–14. [CrossRef]
17. Somna, K.; Jaturapitakkul, C.; Kajitvichyanukul, P.; Chindaprasirt, P. NaOH-Activated Ground Fly Ash Geopolymer Cured at Ambient Temperature. *Fuel* **2011**, *90*, 2118–2124. [CrossRef]
18. De Vargas, A.S.; Dal Molin, D.C.C.; Vilela, A.C.F.; Da Silva, F.J.; Pavão, B.; Veit, H. The Effects of Na_2O/SiO_2 Molar Ratio, Curing Temperature and Age on Compressive Strength, Morphology and Microstructure of Alkali-Activated Fly Ash-Based Geopolymers. *Cem. Concr. Compos.* **2011**, *33*, 653–660. [CrossRef]
19. Robayo-Salazar, R.A.; Mejía-Arcila, J.M.; Mejía de Gutiérrez, R. Eco-Efficient Alkali-Activated Cement Based on Red Clay Brick Wastes Suitable for the Manufacturing of Building Materials. *J. Clean. Prod.* **2017**, *166*, 242–252. [CrossRef]
20. Alhawat, M.; Ashour, A.; Yildirim, G.; Aldemir, A.; Sahmaran, M. Properties of Geopolymers Sourced from Construction and Demolition Waste: A Review. *J. Build. Eng.* **2022**, *50*, 104104. [CrossRef]
21. Wu, H.; Zuo, J.; Zillante, G.; Wang, J.; Yuan, H. Status Quo and Future Directions of Construction and Demolition Waste Research: A Critical Review. *J. Clean. Prod.* **2019**, *240*, 118163. [CrossRef]
22. Provis, J.L.; Duxson, P.; van Deventer, J.S.J. The Role of Particle Technology in Developing Sustainable Construction Materials. *Adv. Powder Technol.* **2010**, *21*, 2–7. [CrossRef]
23. Kvočka, D.; Lešek, A.; Knez, F.; Ducman, V.; Panizza, M.; Tsoutis, C.; Bernardi, A. Life Cycle Assessment of Prefabricated Geopolymeric Façade Cladding Panels Made from Large Fractions of Recycled Construction and Demolition Waste. *Materials* **2020**, *13*, 3931. [CrossRef] [PubMed]
24. Vásquez, A.; Cárdenas, V.; Robayo, R.A.; de Gutiérrez, R.M. Geopolymer Based on Concrete Demolition Waste. *Adv. Powder Technol.* **2016**, *27*, 1173–1179. [CrossRef]
25. Panizza, M.; Natali, M.; Garbin, E.; Tamburini, S.; Secco, M. Assessment of Geopolymers with Construction and Demolition Waste (CDW) Aggregates as a Building Material. *Constr. Build. Mater.* **2018**, *181*, 119–133. [CrossRef]
26. Singh, N.B.; Wali, S.K.; Saxena, S.K.; Kumar, M. Properties of Calcined Clay-Based Geopolymer Mortars in Presence of Alccofine Powder and Recron Fiber. In *RILEM Bookseries*; RILEM: Champs sur Marne, France, 2020. [CrossRef]
27. Hattatoglu, F.; Bakis, A. Usability of Ignimbrite Powder in Reactive Powder Concrete Road Pavement. *Road Mater. Pavement Des.* **2017**, *18*, 1448–1459. [CrossRef]
28. Gimeno, D.; Davidovits, J.; Marini, C.; Rocher, P.; Tocco, S.; Cara, S.; Diaz, N.; Segura, C.; Sistu, C. Desarrollo de Un Cemento de Base Silicatada a Partir de Rocas Volcánicas Vítreas Alcalinas: Interpretatión de Los Resultados Preindustriales Basada En La Compositión Químico- Mineralógica de Los Precursores Geológicos. *Bol. Soc. Esp. Cerám. Vidr.* **2003**, *42*, 69–78. [CrossRef]
29. Duxson, P.; Provis, J.L.; Lukey, G.C.; Mallicoat, S.W.; Kriven, W.M.; Van Deventer, J.S.J. Understanding the Relationship between Geopolymer Composition, Microstructure and Mechanical Properties. *Colloids Surf. A Physicochem. Eng. Asp.* **2005**, *269*, 47–58. [CrossRef]
30. Osio-Norgaard, J.; Gevaudan, J.P.; Srubar, W.V. A Review of Chloride Transport in Alkali-Activated Cement Paste, Mortar, and Concrete. *Constr. Build. Mater.* **2018**, *186*, 191–206. [CrossRef]
31. Askarian, M.; Tao, Z.; Adam, G.; Samali, B. Mechanical Properties of Ambient Cured One-Part Hybrid OPC-Geopolymer Concrete. *Constr. Build. Mater.* **2018**, *186*, 330–337. [CrossRef]
32. Hassan, A.; Arif, M.; Shariq, M. Use of Geopolymer Concrete for a Cleaner and Sustainable Environment—A Review of Mechanical Properties and Microstructure. *J. Clean. Prod.* **2019**, *223*, 704–728. [CrossRef]
33. Ding, Y.; Shi, C.J.; Li, N. Fracture Properties of Slag/Fly Ash-Based Geopolymer Concrete Cured in Ambient Temperature. *Constr. Build. Mater.* **2018**, *190*, 787–795. [CrossRef]
34. Albitar, M.; Mohamed Ali, M.S.; Visintin, P. Evaluation of Tension-Stiffening, Crack Spacing and Crack Width of Geopolymer Concretes. *Constr. Build. Mater.* **2018**, *160*, 408–414. [CrossRef]
35. Mo, K.H.; Alengaram, U.J.; Jumaat, M.Z. Structural Performance of Reinforced Geopolymer Concrete Members: A Review. *Constr. Build. Mater.* **2016**, *120*, 251–264. [CrossRef]

36. Visintin, P.; Mohamed Ali, M.S.; Albitar, M.; Lucas, W. Shear Behaviour of Geopolymer Concrete Beams without Stirrups. *Constr. Build. Mater.* **2017**, *148*, 10–21. [CrossRef]
37. Al-Azzawi, M.; Yu, T.; Hadi, M.N.S. Factors Affecting the Bond Strength Between the Fly Ash-Based Geopolymer Concrete and Steel Reinforcement. *Structures* **2018**, *14*, 262–272. [CrossRef]
38. Castel, A.; Foster, S.J. Bond Strength between Blended Slag and Class F Fly Ash Geopolymer Concrete with Steel Reinforcement. *Cem. Concr. Res.* **2015**, *72*, 48–53. [CrossRef]
39. Albitar, M.; Mohamed Ali, M.S.; Visintin, P.; Drechsler, M. Effect of Granulated Lead Smelter Slag on Strength of Fly Ash-Based Geopolymer Concrete. *Constr. Build. Mater.* **2015**, *83*, 128–135. [CrossRef]
40. Alzeebaree, R.; Çevik, A.; Nematollahi, B.; Sanjayan, J.; Mohammedameen, A.; Gülşan, M.E. Mechanical Properties and Durability of Unconfined and Confined Geopolymer Concrete with Fiber Reinforced Polymers Exposed to Sulfuric Acid. *Constr. Build. Mater.* **2019**, *215*, 1015–1032. [CrossRef]
41. Bouaissi, A.; Li, L.y.; Al Bakri Abdullah, M.M.; Bui, Q.B. Mechanical Properties and Microstructure Analysis of FA-GGBS-HMNS Based Geopolymer Concrete. *Constr. Build. Mater.* **2019**, *210*, 198–209. [CrossRef]
42. Lee, W.H.; Wang, J.H.; Ding, Y.C.; Cheng, T.W. A Study on the Characteristics and Microstructures of GGBS/FA Based Geopolymer Paste and Concrete. *Constr. Build. Mater.* **2019**, *211*, 807–813. [CrossRef]
43. Luhar, S.; Chaudhary, S.; Luhar, I. Development of Rubberized Geopolymer Concrete: Strength and Durability Studies. *Constr. Build. Mater.* **2019**, *204*, 740–753. [CrossRef]
44. Young, R.A. *The Rietveld Method*; Oxford University Press: Oxford, UK, 1993; p. 312.
45. *Bruker AXS TOPAS V6: General Profile and Structure Analysis Software for Powder Diffraction Data*; User's Manual; Bruker AXS: Karlsruhe, Germany, 2017.
46. Zhang, P.; Wang, K.; Li, Q.; Wang, J.; Ling, Y. Fabrication and Engineering Properties of Concretes Based on Geopolymers/Alkali-Activated Binders—A Review. *J. Clean. Prod.* **2020**, *258*, 120896. [CrossRef]
47. Ranjbar, N.; Kuenzel, C.; Spangenberg, J.; Mehrali, M. Hardening Evolution of Geopolymers from Setting to Equilibrium: A Review. *Cem. Concr. Compos.* **2020**, *114*, 103729. [CrossRef]
48. Amran, Y.H.M.; Alyousef, R.; Alabduljabbar, H.; El-Zeadani, M. Clean Production and Properties of Geopolymer Concrete; A Review. *J. Clean. Prod.* **2020**, *251*, 119679. [CrossRef]
49. Samarakoon, M.H.; Ranjith, P.G.; Rathnaweera, T.D.; Perera, M.S.A. Recent Advances in Alkaline Cement Binders: A Review. *J. Clean. Prod.* **2019**, *227*, 70–87. [CrossRef]
50. Piault, P.; King, A.; Henry, L.; Rathore, J.S.; Guignot, N.; Deslandes, J.-P.; Itié, J.-P. A Thresholding Based Iterative Reconstruction Method for Limited-Angle Tomography Data. *Tomogr. Mater. Struct.* **2023**, *2*, 100008. [CrossRef]
51. Bossa, N.; Chaurand, P.; Vicente, J.; Borschneck, D.; Levard, C.; Aguerre-Chariol, O.; Rose, J. Micro- and Nano-X-Ray Computed-Tomography: A Step Forward in the Characterization of the Pore Network of a Leached Cement Paste. *Cem. Concr. Res.* **2015**, *67*, 138–147. [CrossRef]
52. Madsen, I.C.; Scarlett, N.V.Y.; Kern, A. Description and Survey of Methodologies for the Determination of Amorphous Content via X-Ray Powder Diffraction. *Z. Krist.* **2011**, *226*, 944–955. [CrossRef]
53. De Azeredo Melo, L.G.; Pereira, R.A.; Pires, E.F.C.; Darwish, F.A.I.; Da Silva, F.J. Physicochemical Characterization of Pulverized Phyllite Rock for Geopolymer Resin Synthesis. *Mater. Res.* **2017**, *20*, 236–243. [CrossRef]